PCCP

PAPER

View Article Online
View Journal | View Issue

Check for updates

Cite this: *Phys. Chem. Chem. Phys.*, 2024, **26**, 7534

Received 16th November 2023, Accepted 18th January 2024

DOI: 10.1039/d3cp05568j

rsc.li/pccp

Coherent state switching using vibrational polaritons in an asymmetric double-well potential†

Loïse Attal,[a] Florent Calvo,[b] Cyril Falvo[ab] and Pascal Parneix*[a]

The quantum dynamics of vibrational polaritonic states arising from the interaction of a bistable molecule with the quantized mode of a Fabry–Perot microcavity is investigated using a generic asymmetric double-well potential as a simplified one-dimensional model of a reactive molecule. After discussing the role of the light–matter coupling strength in the emergence of avoided crossings between polaritonic states, we investigate the possibility of using these crossings to trigger a dynamical switching of these states from one potential well to the other. Two schemes are proposed to achieve this coherent state switching, either by preparing the molecule in an appropriate vibrational excited state before inserting it into the cavity, or by applying a short laser pulse inside the cavity to obtain a coherent superposition of polaritonic states. The respective influences of dipole moment amplitude and potential asymmetry on the coherent switching process are also discussed.

1 Introduction

Over the recent years, confining molecular systems inside small Fabry–Perot (FP) cavities has been suggested as a way to control their physical and chemical properties.[1–10] Polaritonic chemistry, which exploits the quantization of the electromagnetic field inside such cavities and the resulting hybrid states that arise due to strong light–matter interactions, was first investigated using electronic transitions[1–3] before being extended to vibrational degrees of freedom.[4,5,8,11–14] The so-called polaritonic states could in principle enable greater control over chemical processes such as photoisomerization or reactivity, provided that the entanglement of the light–matter degrees of freedom survives on time scales longer than both the photon lifetime in the cavity and the molecular coherence time.

So far, the changes in the molecular properties caused by vibrational strong coupling (VSC) in a cavity have been probed using various spectroscopy methods, including linear infrared (IR) spectroscopy,[14,15] Raman spectroscopy[11,16–18] as well as 2D-IR spectroscopy.[19–21] Among the various properties that could be altered under VSC, energy transport, photochemical reactivity and thermally driven ground-state chemical reactions have been scrutinized.[15,22–26] However, the difficulties inherent to these experiments[27] have raised a number of controversies regarding their reproducibility[28,29] and interpretation.[27,30]

From a general perspective, and since the vacuum field amplitude E_0 of a confined light mode with frequency ω_c and mode volume V_c is proportional to $1/\sqrt{V_c}$, strong coupling requires the FP cavity to be small, *e.g.* electronic polaritons typically require nanoscale cavities. For vibrational polaritons, since transitions occur in a prescribed electronic state, ω_c typically lies in the range of 10^2–10^3 cm^{-1}, leading to a cavity length $L \approx 1$–10 μm. As shown by the Tavis-Cummings model,[31] the light–matter coupling strength depends on the number N of molecules in the cavity and scales as $\sqrt{N}$, motivating the use of dense media in most experimental studies so far. However, the formation of rovibrational polaritons of gaseous methane confined in a FP microcavity was very recently suggested.[14] Besides allowing larger cavity volumes, diluted media enable much longer photon lifetimes, in excess of the nanosecond for the aforementioned work on methane.

The experimental results on vibrational polaritons have opened a number of fundamental questions that stimulated the interest of the theoretical community,[32–43] aimed at clarifying the role of dissipative effects in the cavity, the importance of dark states and the role of relaxation processes such as intramolecular vibrational relaxation. For single molecules, vibrational polaritons have been extensively studied using simplified models such as Morse potentials[32,34,35,37–39] or symmetric double-well potentials.[37,44] Rovibrational polaritons have also been explored by including two cavity modes with orthogonal polarisation,[41] and particular interest for the possibilities

---

[a] *Université Paris-Saclay, CNRS, Institut des Sciences Moléculaires d'Orsay, 91405 Orsay, France. E-mail: pascal.parneix@universite-paris-saclay.fr*

[b] *Université Grenoble Alpes, CNRS, LIPhy, 38000 Grenoble, France*

† Electronic supplementary information (ESI) available. See DOI: https://doi.org/10.1039/d3cp05568j

offered by multi-mode cavities has recently emerged.[22,45,46] The case of an assembly of confined molecules interacting with each other was also studied, and the importance of dark states on the properties of the polaritonic states was specifically emphasized.[36,42,43,47] However, with the exception of very recent efforts to treat polyatomic molecules fully coupled to the cavity at an *ab initio* level using cavity Born–Oppenheimer models,[48,49] most theoretical studies have relied on quite simplified and low-dimensional models of the molecular systems used in experiments. Such approaches notably struggle to take into account the effects of the environment and the interaction mechanisms between polaritons.

In the present work, and building upon earlier efforts from Triana, Hernandez and coworkers,[34,35,38] we consider a generic one-dimensional asymmetric double-well potential as a simplified model of the electronic ground state of a molecule undergoing a chemical reaction. Under sufficient coupling between the vibrational mode of the molecule and the electromagnetic mode of the cavity, stationary vibrational polaritonic states are formed. These hybrid light–matter states exhibit avoided crossings at specific values of the coupling strength that are used to trigger a coherent state switching between the two wells of the asymmetric potential. The localization of some polaritonic states in one potential well or the other is made possible by the asymmetry of the potential, which lifts the symmetry constraints that prevented the localization of the eigenstates in symmetric potentials. Different ways of altering the polaritonic states to induce coherent switching are considered, either by preparing the molecule in a specific vibrational state before inserting it into the cavity or by exposing the hybrid system to an external picosecond laser pulse. An efficient coherent state switching between vibrational polaritons located in each potential well is numerically observed for suitable values of the light–matter coupling strength.

In Section 2, the theoretical framework used to describe the one-dimensional model system and its interaction with the microcavity is presented, and some computational details are provided. The computational results are presented and discussed in Section 3, first for stationary states and then under the two out-of-equilibrium aforementioned conditions. Section 4 concludes the article by summarizing the main results and opening some perspectives for future efforts.

2 Theory

2.1 Hamiltonian

We consider a single molecule ($N = 1$) described by a simple one-dimensional model with coordinate q and momentum p, in vibrational strong coupling with a single-mode FP microcavity. The Pauli–Fierz Hamiltonian[50] describing such a molecule interacting with the quantized electromagnetic mode of the cavity is given by

$$H = H_{\text{cav}} + H_{\text{mol}} + H_{\text{int}}, \tag{1}$$

in which H_{cav}, H_{mol} and H_{int} denote the contributions of the cavity, of the molecule, and of their interaction, respectively. Without loss of generality, the vibrational Hamiltonian of the molecule is given by

$$H_{\text{mol}}(q,p) = \frac{p^2}{2\mu} + V(q), \tag{2}$$

with μ the reduced mass of the molecule and $V(q)$ its potential energy operator. This Hamiltonian can be diagonalized to obtain the free molecule vibrational eigenstates $|v\rangle$ and their associated energies $E(v) = \omega_v$, omitting here and below the factor $\hbar$.

The single-mode cavity Hamiltonian, which is characterized by its mode frequency ω_c, can be written using the creation and annihilation operators as

$$H_{\text{cav}} = \omega_c a^\dagger a. \tag{3}$$

The cavity mode frequency is chosen to be in resonance with the fundamental molecular transition to ensure a strong light–matter interaction. This interaction depends on the vacuum field amplitude $E_0 = \sqrt{\omega_c / V_c \varepsilon_0}$ and on the dipole moment d of the molecule. In the following, the rotation of the molecule is neglected, and the dipole moment vector is assumed to be aligned with the polarization vector of the cavity mode. This allows us to only consider scalar quantities in the coupling Hamiltonian. By taking into account both the dipolar interaction and the dipole self-energy contribution,[37] the molecule-light interaction can be written as

$$H_{\text{int}} = E_0 d\left(a^\dagger + a\right) + \frac{{E_0}^2}{\omega_c} d^2. \tag{4}$$

The strength of this coupling can be characterized by the dimensionless parameter λ_c given by

$$\lambda_c = \frac{E_0 |d_{01}|}{\omega_c}, \tag{5}$$

with $d_{01} = \langle 0|d|1\rangle$ the dipole moment between the ground and the first vibrational excited state of the molecule.

Using the vibrational eigenstates $|v\rangle$ of the free molecule and the cavity mode Fock states $|n\rangle$, the Pauli–Fierz Hamiltonian can be expressed in the uncoupled basis set $|v,n\rangle = |v\rangle \otimes |n\rangle$ as

$$\begin{aligned} H \; = \; & \sum_n \sum_v (n\omega_c + \omega_v)|v,n\rangle\langle v,n| \\ & + \lambda_c \omega_c \sum_n \sum_v \sum_{v'} \frac{\langle v'|d|v\rangle}{|d_{01}|}(|v',n+1\rangle\langle v,n| + |v',n\rangle\langle v,n+1|) \\ & + {\lambda_c}^2 \omega_c \sum_n \sum_v \sum_{v'} \frac{\langle v'|d^2|v\rangle}{{d_{01}}^2}|v',n\rangle\langle v,n|, \end{aligned} \tag{6}$$

where eqn (5) was used to introduce the coupling parameter λ_c in the Hamiltonian.

2.2 Asymmetric double-well potential

The vibrational Hamiltonian assumes the following asymmetric double-well potential mimicking a bistable molecule

$$V(q) = \alpha_0 q^4 - \alpha_1 q^2 + \alpha_2 q, \tag{7}$$

Table 1 Parameters chosen for the potential energy and dipole moment functions. The numbers N_ℓ and N_r of vibrational states localized in the two wells of the potential are also reported

α_0 (a.u.)	α_1 (a.u.)	α_2 (a.u.)	ω_{01} (cm^{-1})	N_ℓ	N_r
1/2048	1/256	2×10^{-3}	557	6	2

γ_1 (a.u.)	δ_1 (a.u.)	γ_2 (a.u.)	δ_2 (a.u.)
1	2	1	2

in which $\alpha_0 > 0$, $\alpha_1 > 0$ and α_2 are three parameters. The positions of the two local minima of this double-well potential are denoted as q_1 and $q_2 > q_1$. In the case of a symmetric potential ($\alpha_2 = 0$), these equilibrium positions are found at $q_2 = -q_1 = \sqrt{\alpha_1/2\alpha_0}$. As we are mainly interested in the phenomenology of polaritonic chemistry, we have chosen to use values for these quantities that are not related to any particular chemical system but yield molecular positions, transition frequencies, and depths of the potential wells that are in the same orders of magnitude as realistic molecules, namely Angströms, hundreds of cm^{-1}, and fractions of eVs. These values, reported in Table 1, yield the potential energy curve represented in Fig. 1(a). The discrete variable representation (DVR)[51,52] was used to solve the 1D time-independent Schrödinger equation and determine the first bound states of the double-well asymmetric potential, assuming the same reduced mass of μ = 1.43 amu as employed by Triana *et al.*[35] With the current parameters, the vibrational frequency ω_{01} of the deepest well is found at 557 cm^{-1}, the second well having a lower fundamental frequency of 422.5 cm^{-1}. The bound states of the asymmetric potential are also depicted in Fig. 1(a) with different colors for the two wells. Following this representation, the two wells will be referred to as left (ℓ) and right (r). The vibrational states corresponding to the left (resp. right) well will be denoted as v_ℓ (resp. v_r). With the current parameters, the left well is the deepest one and supports $N_\ell = 6$ vibrational states, while the right well contains $N_r = 2$ states. Higher vibrational states spread over the barrier and are not exclusively confined to either well. The cavity mode being in resonance with the first allowed vibrational transition, it corresponds to the transition between the two first levels of the left well, *i.e.* $\omega_c = \omega_{01} = 557$ cm^{-1}.

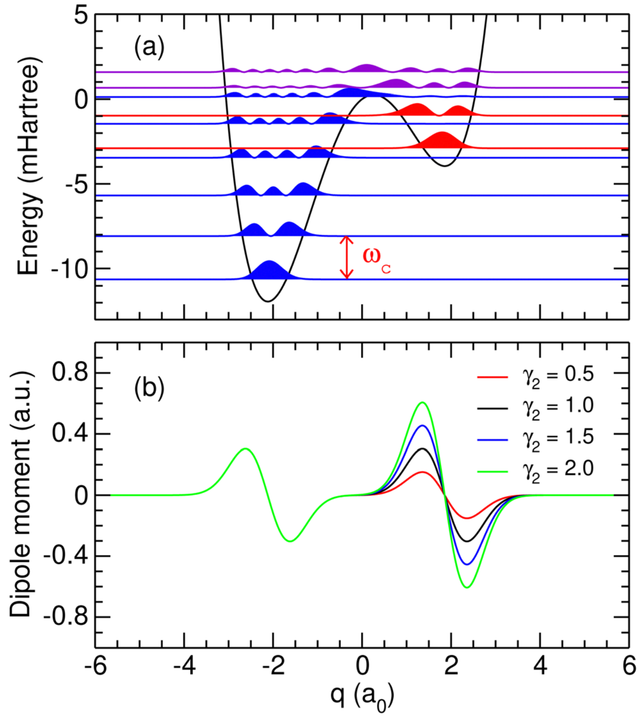

Fig. 1 (a) Potential energy curve and probability densities of the ten lowest molecular eigenstates obtained using the parameters given in Table 1. Probability densities located in the left or right well are represented in blue and red, respectively, while the densities spreading over the barrier are represented in purple; (b) dipole moment functions obtained using the parameters given in Table 1 and several values of γ_2 given in atomic units.

2.3 Dipole moment function

To describe the light–matter interaction, we assume for simplicity that the molecule is non-polar in both wells and extend the work of Hernandez and Herrera[34] to a double well-potential to obtain the empirical dipole moment function

$$d(q) = -\gamma_1(q - q_1)\mathrm{e}^{-\delta_1(q-q_1)^2} - \gamma_2(q - q_2)\mathrm{e}^{-\delta_2(q-q_2)^2}, \qquad (8)$$

with γ_k and δ_k some (strictly positive) parameters for k = 1,2. This functional form is appropriate for a molecular system that is nonpolar in the vicinity of both potential wells [$d(q_k) = 0$ for k = 1, 2], and it is also well-behaved with respect to a number of physically expected rules such as being maximum at a finite coordinate around equilibrium and vanishing at long distance.[34] The polarizability γ_k measuring the dipole gradient at the corresponding minimum q_k and governing the dipole amplitude in the associated well is an adjustable parameter. Using the values reported in Table 1, the variations of the dipole moment function with coordinate q are shown in Fig. 1(b). In the following, the reference dipole moment function will be the one defined by $\gamma_2 = \gamma_1 = 1.0$ a.u. Other dipole moment functions obtained with alternative values of γ_2 are displayed in Fig. 1(b). As the ratio γ_2/γ_1 governs the relative excitation probabilities in the left and the right wells, the sensitivity of our results with respect to this ratio will later be investigated.

2.4 Polaritonic state properties

The hybrid light–matter polaritonic states $|P_i\rangle$ are obtained by diagonalization of the total Hamiltonian H using a finite number of vibrational states N_v and photonic states N_p. These states can be written in the uncoupled basis set $|v,n\rangle$ as

$$|P_i\rangle = \sum_{v=0}^{N_v-1}\sum_{n=0}^{N_\mathrm{p}-1} c_{v,n}^{(i)}|v,n\rangle. \qquad (9)$$

The associated eigenenergies will be denoted as ε_i. The vibrational polaritonic states themselves are more conveniently characterized by appropriate averaging and projecting over light or matter degrees of freedom. For each polaritonic state,

$|P_i\rangle$, the mean value of q, noted $\langle q\rangle_i$ and the average number of photons $\langle n_\mathrm{p}\rangle_i$ are computed as

$$\langle q\rangle_i = \langle P_i|q|P_i\rangle, \tag{10}$$

$$\langle n_\mathrm{p}\rangle_i = \langle P_i|\tilde{a}^\dagger\tilde{a}|P_i\rangle. \tag{11}$$

The assignment of a given polaritonic state $|P_i\rangle$ within one of the two wells (ℓ or r) is obtained from the value of $\langle q\rangle_i$. For a symmetric well, the top of the barrier separating the two wells is at $q = 0$; therefore, the left well is characterized by $\langle q\rangle < 0$ and the right one by $\langle q\rangle > 0$. This remains essentially true for the asymmetric well considered here as the top of the barrier is only shifted by about 0.26 bohr. The sign of $\langle q\rangle_i$ will thus be used to determine the localization of the associated polariton $|P_i\rangle$.

2.5 Infrared spectroscopy

The strength of the radiative coupling between two polaritonic states $|P_i\rangle$ and $|P_j\rangle$ can be characterized by

$$R_{i,j} = \left|\frac{\langle P_i|d|P_j\rangle}{\langle 0_\ell|d|1_\ell\rangle}\right|^2, \tag{12}$$

where, as in eqn (6), we choose to normalize the coupling between the two polaritons by the corresponding radiative coupling of the first IR transition.

At thermal equilibrium, the state of the confined system can be probed using IR spectroscopy. Denoting by $\beta = 1/k_\mathrm{B}T$, the inverse temperature (with k_B the Boltzmann constant), the linear absorption intensity obtained with a laser excitation at frequency ω and characterized by a Gaussian spectral profile can be estimated by

$$I_\beta(\omega) \propto \sum_i \sum_{j>i} \frac{\left(\mathrm{e}^{-\beta\varepsilon_i} - \mathrm{e}^{-\beta\varepsilon_j}\right)}{Z(\beta)} R_{i,j} \times g(\omega - \omega_{ij}) \tag{13}$$

with $\omega_{ij} = \varepsilon_j - \varepsilon_i$, $Z(\beta)$ the canonical partition function and $g(\omega - \omega_{ij})$ the Gaussian broadening function centered at ω_{ij}. The IR absorption spectrum depends on the coupling parameter λ_c through the eigenenergies ε_i and the radiative couplings $R_{i,j}$. The spectral response of the hybrid system is given by eqn (13) only if the polaritonic state relaxation time is longer than the temporal profile of the laser excitation.

2.6 Polaritonic state evolution

The time evolution of an initial non-stationary state, denoted as $|\Psi(t = 0)\rangle$, can be obtained by solving the time-dependent Schrödinger equation (TDSE) at a given value of the coupling parameter λ_c. From a unitary transformation, the initial wavepacket can be decomposed linearly over the polaritonic states as

$$|\Psi(t=0)\rangle = \sum_i b_i(0)|P_i\rangle, \tag{14}$$

where the coefficients $b_i(0)$ depend on λ_c. The time evolution of the wavepacket is then governed by the TDSE, which can be solved exactly in the polaritonic basis set as the Hamiltonian does not explicitly depend on time. The wavepacket at time t is more conveniently expressed in the uncoupled basis set as

$$|\Psi(t)\rangle = \sum_{v=0}^{N_v-1} \sum_{n=0}^{N_\mathrm{p}-1} \underbrace{\sum_k b_k(0)\mathrm{e}^{-i\varepsilon_k t} c_{v,n}^{(k)}}_{A_{v,n}(t)} |v,n\rangle, \tag{15}$$

where $|A_{v,n}(t)|^2$ corresponds to the probability for the system to lie in the uncoupled state $|v,n\rangle$ at time t. The mean values $\langle q\rangle(t) = \langle\Psi(t)|q|\Psi(t)\rangle$ and $\langle n_\mathrm{p}\rangle(t) = \langle\Psi(t)|a^\dagger a|\Psi(t)\rangle$ can be computed along the trajectory to analyze the position of the system inside the potential wells and the number of photons in the cavity, respectively.

3 Results and discussion

All results presented below were obtained for a single molecule ($N = 1$) with a maximum number of $N_v = 40$ vibrational states and $N_\mathrm{p} = 40$ photons. These values ensure convergence for the polaritonic states studied here. Unless otherwise specified, the parameters used for the potential function are those reported in Table 1, notably $\gamma_2 = \gamma_1 = 1.0$ a.u.

3.1 Avoided crossings and polariton localization

The role of the coupling parameter λ_c on vibrational polaritonic states is first discussed, with Fig. 2 showing the variations of their eigenenergies (relative to the ground polaritonic state) with increasing values of λ_c. At each value of the coupling parameter, the polaritonic states $|P_i\rangle$ are ordered by increasing energy. Since the investigated system features some true crossings, the label i associated with a given physical state may

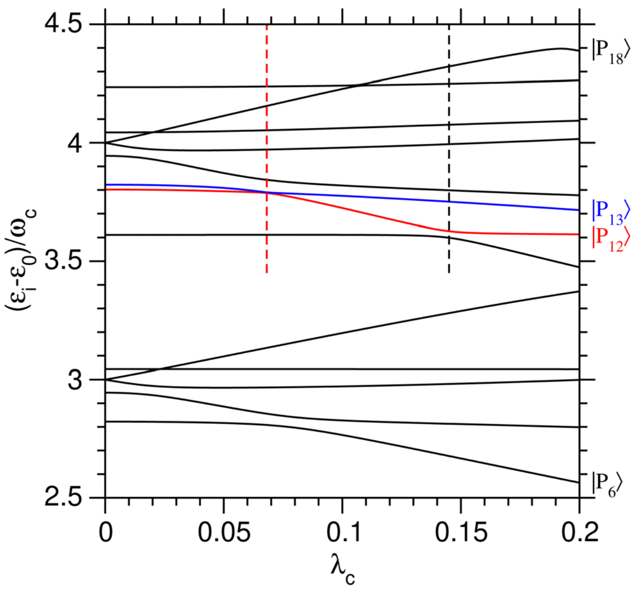

Fig. 2 Eigenenergies of the polaritonic states $|P_i\rangle$, i = 6–18, lying in the region near $3\omega_\mathrm{c}$ and $4\omega_\mathrm{c}$ above the ground polaritonic state, as a function of the coupling strength λ_c. The eigenenergies of states $|P_{12}\rangle$ and $|P_{13}\rangle$ are highlighted in red and blue, respectively. The dashed vertical lines highlight the two avoided crossings involving the pairs ($|P_{11}\rangle$,$|P_{12}\rangle$) and ($|P_{12}\rangle$,$|P_{13}\rangle$) and occurring at λ_c = 0.145 and 0.068, respectively.

change depending on the value of λ_c. To study the coherent switching between the two wells, we focus on the energy range where both potential wells exist, while remaining below the barrier. As seen from Fig. 1(a), this typically corresponds to energies between $3\omega_c$ and $4\omega_c$ above the ground state. As shown by the corresponding assignments in Table 2, at $\lambda_c = 0$, five polaritonic states ($|P_i\rangle$ for $i = 6$–10) are located near $3\omega_c$, while eight states ($i = 11$–18) reside near $4\omega_c$. In this range, the eigenenergies of the polaritonic states are found to be generally sensitive to λ_c, with neighboring states often exhibiting avoided crossings.

As seen in Fig. 2, several polaritonic states are doubly degenerated at $\lambda_c = 0$, as the consequence of the exact resonance condition between ω_c and the first vibrational transition of the left potential well being met. As an example, $|P_8\rangle$ and $|P_9\rangle$ share the same energy at $\lambda_c = 0$ as they correspond to $|0_\ell,3\rangle$ and $|1_\ell,2\rangle$, respectively (see Table 2). Note that the energies of states $|2_\ell,1\rangle$ and $|3_\ell,0\rangle$ are shifted from the doubly degenerated value due to the anharmonicity of the potential well, which causes a detuning between the cavity mode frequency and the vibrational hot bands. A similar degeneracy occurs between $|P_{15}\rangle$ and $|P_{16}\rangle$, which, respectively, correspond to $|0_\ell,4\rangle$ and $|1_\ell,3\rangle$ at $\lambda_c = 0$.

Several avoided crossings are also visible in Fig. 2. As discussed in ref. 34, they occur when the main contributions in the $|\nu,n\rangle$ basis set of the two polaritonic states involved are characterized by $|\Delta n| = 1$. Near $3\omega_c$, avoided crossings involve the ($|P_6\rangle$, $|P_7\rangle$) pair at $\lambda_c \simeq 0.08$, as well as the ($|P_7\rangle$, $|P_8\rangle$) pair at $\lambda_c \simeq 0.02$. The decomposition of these three polaritonic states in the uncoupled basis set shows that they only involve vibrational states sitting in the left potential well ($\langle q\rangle_i < 0$ for all values of λ_c), making those avoided crossings unsuitable to achieve coherent a switching between the two wells.

Two other avoided crossings can be found around $4\omega_c$: between $|P_{12}\rangle$ and $|P_{13}\rangle$ at $\lambda_c = 0.068$ and between $|P_{11}\rangle$ and $|P_{12}\rangle$ at $\lambda_c = 0.145$. Fig. 3 focuses on the ($|P_{12}\rangle$, $|P_{13}\rangle$) pair and shows the variations of several properties associated with these two polaritonic states when λ_c increases, starting with their relative energies in Fig. 3(a). The corresponding variations of the average position $\langle q\rangle_i$ and photon number $\langle n_p\rangle_i$ are represented in panels (b) and (c) of the same figure. The first avoided crossing occurs at $\lambda_{crit} = 0.068$ where the energy difference between $|P_{12}\rangle$ and $|P_{13}\rangle$ is as small as $\Delta\varepsilon_{crit}/\omega_c \approx 3 \times 10^{-3}$. As seen in Fig. 3(b), the system effectively switches between the two wells near this avoided crossing, with simultaneous switching of $|P_{12}\rangle$ from the right well ($\langle q\rangle_{12} > 0$ for $\lambda_c < \lambda_{crit}$) to the left well ($\langle q\rangle_{12} < 0$ for $\lambda_c > \lambda_{crit}$) and of $|P_{13}\rangle$ from left to right. The avoided crossing also strongly alters the average number of photons $\langle n_p\rangle$ in the two polaritonic states with $|P_{12}\rangle$ suddenly gaining two photons and $|P_{13}\rangle$ losing one photon.

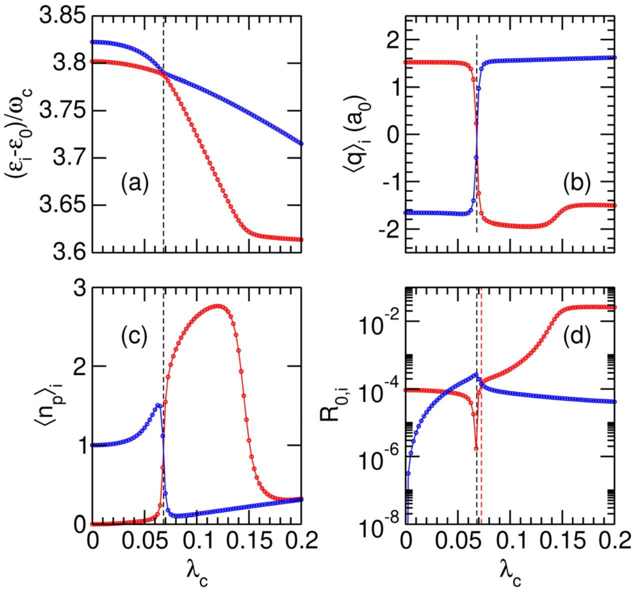

Fig. 3 Variations of stationary properties of the polaritonic states $|P_i\rangle$ for $i = 12$ (red) and $i = 13$ (blue) with increasing coupling strength λ_c. (a) Relative energies $(\varepsilon_i - \varepsilon_0)/\omega_c$; (b) average position $\langle q\rangle_i$ along the potential wells; (c) average number of photons $\langle n_p\rangle_i$; (d) normalized radiative coupling strength $R_{0,i}$. In the four panels, the black vertical dashed lines highlight the position of the avoided crossing at $\lambda_c = \lambda_{crit}$. In panel (d), the red vertical dashed line at $\lambda_c = \lambda_R$ highlights the coupling strength at which $R_{0,12} = R_{0,13}$.

Table 2 Assignement of the polaritonic states ($|P_i\rangle$, $i = 6$–18) for $\lambda_c = 0$. The symbols ℓ and r correspond to vibrational states localized in the left and right potential wells, respectively

Polariton $|P_i\rangle$	$\varepsilon_i - \varepsilon_0 \sim 3\omega_c$ $|\nu,n\rangle$	$\varepsilon_i - \varepsilon_0 \sim 4\omega_c$ $|\nu,n\rangle$
$|P_6\rangle$	$|3_\ell,0\rangle$	
$|P_7\rangle$	$|2_\ell,1\rangle$	
$|P_8\rangle$	$|1_\ell,2\rangle$	
$|P_9\rangle$	$|0_\ell,3\rangle$	
$|P_{10}\rangle$	$|0_r,0\rangle$	
$|P_{11}\rangle$		$|4_\ell,0\rangle$
$|P_{12}\rangle$		$|1_r,0\rangle$
$|P_{13}\rangle$		$|3_\ell,1\rangle$
$|P_{14}\rangle$		$|2_\ell,2\rangle$
$|P_{15}\rangle$		$|1_\ell,3\rangle$
$|P_{16}\rangle$		$|0_\ell,4\rangle$
$|P_{17}\rangle$		$|0_r,1\rangle$
$|P_{18}\rangle$		$|5_\ell,0\rangle$

The avoided crossing between $|P_{11}\rangle$ and $|P_{12}\rangle$ at $\lambda_c = 0.145$ induces only a minor shift in the energy and average position of the $|P_{12}\rangle$ state [see Fig. 3(a) and (b)]. In particular, the system does not switch between the two wells at this value of the coupling strength ($\langle q\rangle_{12}$ does not change sign) as both $|P_{11}\rangle$ and $|P_{12}\rangle$ reside in the left well when approaching $\lambda_c = 0.145$. Only the photon number varies significantly near $\lambda_c = 0.145$, thus suggesting that this avoided crossing is due to a photon exchange between $|P_{11}\rangle$ and $|P_{12}\rangle$ rather than a coherent switching between the two wells.

To better understand the evolution of the system near the avoided crossing at $\lambda_{crit} = 0.068$, which is the only one leading to a switching between the two wells, we consider the decomposition of polaritonic states $|P_{12}\rangle$ and $|P_{13}\rangle$ in the $|\nu,n\rangle$ basis set. The weights of $|P_{12}\rangle$ and $|P_{13}\rangle$ on different uncoupled states are given in Fig. 4 as a function of λ_c. The distribution of the polaritonic states among the two potential wells is found to vary abruptly near λ_{crit}, highlighting the extreme sensitivity of the

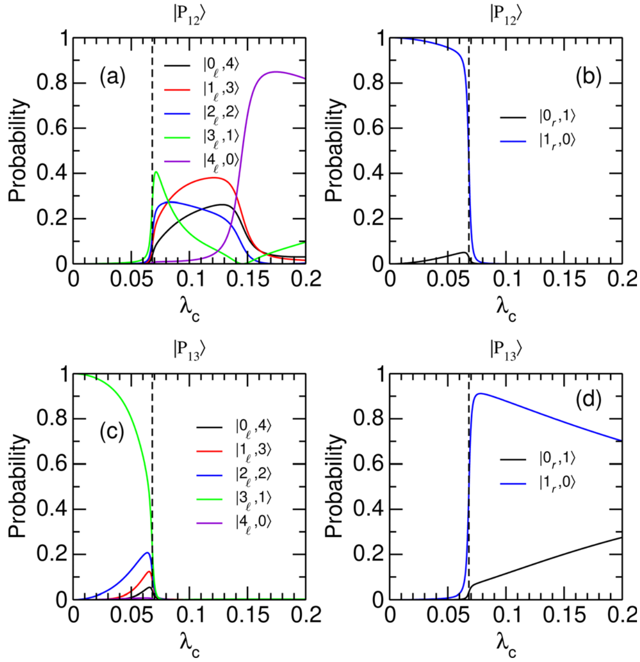

Fig. 4 Probabilities for polaritonic states $|P_i\rangle$, i = 12 and 13 to be in the uncoupled states $|v_{\ell/r},n\rangle$, as a function of the coupling strength λ_c. (a) and (b) $|\langle v,n|P_{12}\rangle|^2$; (c) and (d) $|\langle v,n|P_{13}\rangle|^2$. Uncoupled states that belong to the left (right) well are shown in the left (right) panels. The vertical dashed lines highlight the position of the avoided crossing at $\lambda_c = \lambda_{\text{crit}}$.

coherent switching process to the strength of the light–matter coupling. As λ_c crosses λ_{crit} from below, the polaritonic state $|P_{12}\rangle$, which mostly involves the first excited state of the right well with no additional photon ($|1_r,0\rangle$), turns into a mixture of vibrationally excited states of the left well with v_ℓ = 0–4 and a complementary number $n_p = 4 - v_\ell$ of photons [see Fig. 4(a) and (b)]. The significant weights carried by states with $n_p > 1$ explain the sudden increase in the average number of photons of $|P_{12}\rangle$ found in Fig. 3(c). Concomitantly, the polaritonic state $|P_{13}\rangle$ that occupied the left well in its third vibrationally excited state with one photon in the cavity ($|3_\ell,1\rangle$) is entirely transferred to the right well as a superposition of states $|1_r,0\rangle$ and $|0_r,1\rangle$ [see Fig. 4(c) and (d)]. This superposition is first dominated by the $|1_r,0\rangle$ state while state $|0_r,1\rangle$ gains in weight as λ_c increases. This trend is consistent with the evolution of the average number of photons in $|P_{13}\rangle$ reported in Fig. 3(c).

Considering the strong sensitivity of this phenomenon with respect to the coupling strength, the influence of the dipole moment function was also addressed by changing the value of γ_2 in eqn (8), leaving the other parameters unaffected. The same phenomenology was obtained for all the studied values of γ_2, and the critical coupling strengths λ_{crit} computed for γ_2 varying in the range 0.5–2.0 a.u. are given in Table 3. Since γ_2 governs the dipole moment amplitude in the right well, the states $|0_r,1\rangle$ and $|1_r,0\rangle$ become increasingly coupled as this parameter increases. For small values of the coupling strength ($\lambda_c < \lambda_{\text{crit}}$), the state $|1_r,0\rangle$ is the main component of polariton $|P_{12}\rangle$ [see Fig. 4(b)] and $|0_r,1\rangle$ is a major component of $|P_{17}\rangle$. The increasing coupling between these two states leads them to repel one another, and since $|P_{17}\rangle$ has a higher energy than $|P_{12}\rangle$, this stabilizes $|P_{12}\rangle$ by lowering its energy. In contrast, the polaritonic state $|P_{13}\rangle$ remains mostly unaffected as it lies in the left well. As seen in Table 3, this leads to an increase in the critical value λ_{crit} of the avoided crossing upon increasing γ_2. We also find that the energy difference $\Delta\varepsilon_{\text{crit}}$ at the critical coupling strength decreases with increasing values of γ_2. Above the avoided crossing ($\lambda_c > \lambda_{\text{crit}}$) $|P_{12}\rangle$ and $|P_{13}\rangle$ switch between wells, hence for larger coupling strengths $|P_{12}\rangle$ is no longer affected by the value of γ_2 while $|P_{13}\rangle$ is stabilized when this parameter increases.

Table 3 Critical coupling strengths λ_{crit} and λ_R involving the polaritonic states $|P_{12}\rangle$ and $|P_{13}\rangle$, as computed for increasing values of γ_2. The energy gaps $\Delta\varepsilon_{\text{crit}}/\omega_c$ and $\Delta\varepsilon_R/\omega_c$ refer to the energy difference between these two polaritonic states when $\lambda_c = \lambda_{\text{crit}}$ and $\lambda_c = \lambda_R$, respectively

γ_2 (a.u.)	λ_{crit} ($\times10^{-3}$)	$\Delta\varepsilon_{\text{crit}}/\omega_c$ ($\times10^{-3}$)	λ_R ($\times10^{-3}$)	$\Delta\varepsilon_R/\omega_c$ ($\times10^{-3}$)
0.50	61.9	2.8	67.8	7.7
0.75	64.4	2.8	69.7	7.0
1.00	68.1	2.7	72.5	6.2
1.25	72.5	2.6	76.3	5.3
1.50	78.1	2.4	81.3	4.6
1.75	85.0	2.2	87.2	3.7
2.00	92.8	2.1	94.4	3.0

Finally, the radiative coupling $R_{0,i}$ between the polaritonic ground state $|P_0\rangle$ and a given $|P_i\rangle$ (i = 12, 13) state is displayed in Fig. 3(d) as a function of increasing coupling strength λ_c. In the limit of small values of λ_c, the radiative coupling ratios $R_{0,12}$ and $R_{0,13}$ converge toward the values in the free molecule, namely $|\langle 0_\ell|d|1_r\rangle|^2/|\langle 0_\ell|d|1_\ell\rangle|^2 \simeq 10^{-4}$ for the $|P_{12}\rangle$ state and $\langle 0_r,0|d|3_\ell,1\rangle = \langle 0_r|d|3_\ell\rangle \times \langle 0|1\rangle = 0$ for the $|P_{13}\rangle$ state.

At higher values of λ_c, and especially near the critical coupling strength λ_{crit}, the variations of the radiative coupling are quite strong [notice the logarithmic scale in Fig. 3(d)]. Another interesting feature is found for $\lambda_c = 0.0725 = \lambda_R$ at which the two states $|P_{12}\rangle$ and $|P_{13}\rangle$ share the same radiative coupling strength. This particular value of λ_c is important since it allows the system to be prepared as a coherent superposition of these two polaritonic states, thus allowing some manipulation with a laser field. This possibility will be explored further and discussed in Section 3.2.2. The values of λ_R and the corresponding energy gaps $\Delta\varepsilon_R$ are also reported in Table 3 as a function of increasing γ_2. As is the case with λ_{crit}, λ_R increases with γ_2, owing to greater resulting coupling in the right well. The associated energy gap $\Delta\varepsilon_R$ is found to decrease when γ_2 increases, which we speculatively interpret as the consequence of the avoided crossing becoming increasingly sharper with increasing transition dipole moment.

3.2 Coherent state switching

3.2.1 Starting from a free-excited molecule. We first consider a molecule prepared in a specific vibrational excited state $|v = 1_r\rangle$ and that enters the initially photonless cavity (n_p = 0) at time t = 0, leading to the initial state $|1_r,0\rangle$. The coupling strength is taken at the critical value $\lambda_c = \lambda_{\text{crit}}$ of the avoided crossing discussed above. At this value of the coupling strength, the two polaritonic states $|P_{12}\rangle$ and $|P_{13}\rangle$ involved in the possible switching have a nonzero contribution on the initial $|1_r,0\rangle$ state (see Fig. 4). As seen in Fig. 5(a) for several dipole function parameters γ_2, the initial state is almost a linear combination of $|P_{12}\rangle$ and $|P_{13}\rangle$. This is especially true for small values of γ_2 where the mixing with other polaritonic states residing in the right well is minimal.

The time evolution of the wavepacket in the initially photonless cavity is then followed by numerically solving the TDSE, starting from $|1_r,0\rangle$. The effects of inserting the molecule in the microcavity at $\lambda_c = \lambda_{crit}$ are particularly spectacular with the system alternatively switching between the two wells with a period ranging from around 2200 to 3000 $\omega_c t$, which using the parameters of Table 1 corresponds to 20–30 ps, depending on the value of γ_2. This can be seen from the variations of $\langle q\rangle(t)$ displayed in Fig. 5(b). Note that when varying γ_2, the values of the coupling strength were adjusted to the corresponding critical values λ_{crit} as given in Table 3.

By increasing γ_2, the switching becomes less efficient and is associated with a longer period, as well as more significant fluctuations that are a manifestation of the importance of polaritonic states other than $|P_{12}\rangle$ and $|P_{13}\rangle$ in the decomposition of the initial state. The histogram of Fig. 5(a) reveals that these additional contributions are mostly due to state $|P_{16}\rangle$, which plays an important role when γ_2 increases and thus contributes to the additional high-frequency oscillations seen in Fig. 5(b). At $\lambda_c = 0$, $|P_{16}\rangle$ is referred to as $|P_{17}\rangle$ due to the true crossing occurring between $\lambda_c = 0$ and λ_{crit} and corresponds to the uncoupled state $|0_r,1\rangle$. However, it progressively gains weight on state $|1_r,0\rangle$ as λ_c increases. The coupling between these two states being stronger when the dipole moment in the right well increases, the weight of polaritonic state $|P_{16}\rangle$ in the decomposition of the initial state $|1_r,0\rangle$ increases with γ_2.

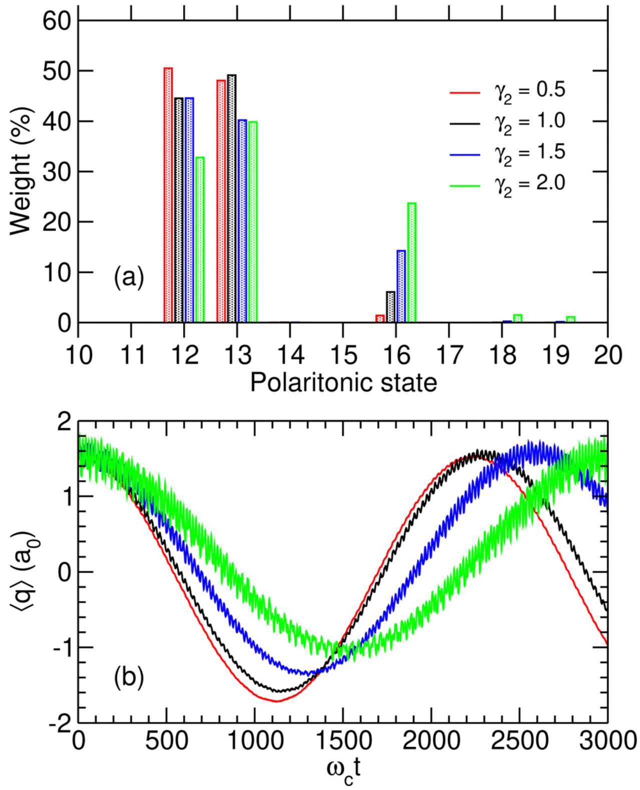

Fig. 5 (a) Initial weights $|b_i(0)|^2$ of the polaritonic states $|P_i\rangle$ for i = 10–20 and for four values of γ_2 given in atomics units; (b) average position $\langle q\rangle$ as a function of time for $\lambda_c = \lambda_{crit}$, assuming the system is initiated at t = 0 in the state $|1_r,0\rangle$, for the same values of γ_2.

The situation considered here of the specific preparation of the system as it enters the microcavity is experimentally challenging, as it would typically require the molecules to be prepared in a uniformly excited flow perpendicular to the cavity axis. However, such experiments could be used to prepare molecules in either well of a bistable potential by adjusting their interaction time with the confined light. This could be done, *e.g.*, by tuning the velocity of the molecular flow in order to synchronize the interaction time with the polaritonic oscillation period, and might enable a higher degree of control of the system state at the output of the cavity. As far as photon lifetimes are concerned, the switching period found with this model system would be far too long for liquid phase experiments but is compatible with measurements in the gas phase.[14]

3.2.2 Using a short IR laser pulse. As an alternative to the preparation of a specific vibrational state outside of the cavity, we now consider the possibility of acting on a system in thermal equilibrium inside the FP cavity through an external excitation using a short IR laser pulse. From Fig. 3(d), the radiative couplings $R_{0,12}$ and $R_{0,13}$ are found to cross each other at a coupling strength of λ_R = 0.0725 slightly higher than the critical value λ_{crit} at which the corresponding eigenenergies cross. At this higher coupling strength, the radiative excitation probabilities from the ground polaritonic state towards $|P_{12}\rangle$ or $|P_{13}\rangle$ become identical. This very specific situation can be exploited to trigger a dynamical coherent switching between the polaritonic states $|P_{12}\rangle$ and $|P_{13}\rangle$ by preparing the system in an equal superposition of these two states using a short laser pulse:

$$|\Psi(t=0)\rangle \simeq \frac{1}{\sqrt{2}}(|P_{12}\rangle + |P_{13}\rangle). \tag{16}$$

However, efficient switching requires strict control of this initial state, which may be difficult to achieve at high temperatures. Temperature effects were investigated specifically by calculating the IR absorption spectra at two temperatures T such that k_BT/ω_c = 0.05 and 0.15, corresponding to about 40 and 120 K, respectively. Calculations were conducted with the set of parameters reported in Table 1, including γ_2 = 1.0 a.u., and at the coupling strength $\lambda_c = \lambda_R$. The relative IR absorption intensities obtained from eqn (13) and normalized by the intensity of the $\nu = 0_\ell \rightarrow 1_\ell$ transition of the free molecule are shown in Fig. 6 at these two temperatures. At $T = 0.05\omega_c/k_B$, only transitions starting from the ground polaritonic state can be distinguished. The most intense transition is found at $\omega/\omega_c \approx 3.6$ and corresponds to the overtone transition $\nu = 0_\ell \rightarrow 4_\ell$ that connects the ground polaritonic states $|P_0\rangle$ to the excited state $|P_{11}\rangle$. The two transitions leading from $|P_0\rangle$

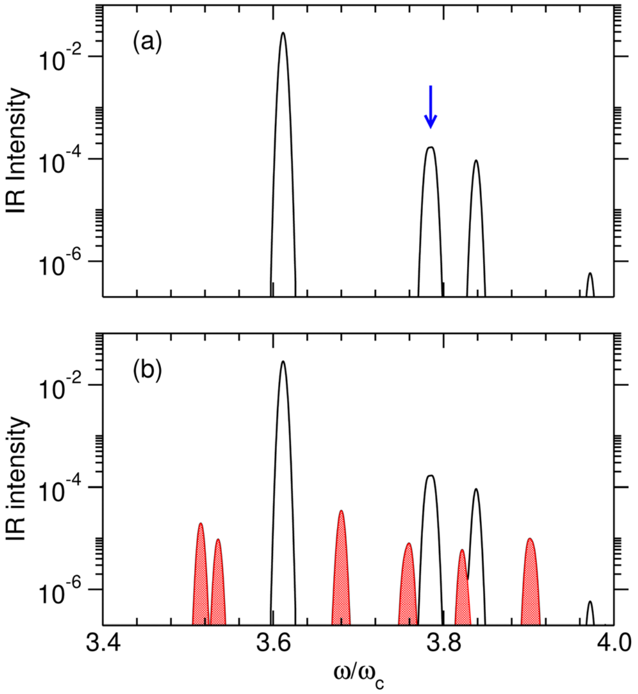

Fig. 6 Relative IR absorption intensity of the polaritonic system at thermal equilibrium obtained at the coupling strength $\lambda_c = \lambda_R$, and for γ_2 = 1.0 a.u. (a) $T = 0.05\omega_c/k_B$. The blue arrow highlights the excitation corresponding to the (almost identical) eigenenergies of the polaritonic states $|P_{12}\rangle$ and $|P_{13}\rangle$; (b) $T = 0.15\omega_c/k_B$. The transitions corresponding to hot bands are shown in red. In both panels, the absorption spectra were convoluted with a Gaussian function having full width at half maximum of 4 cm^{-1}.

to either $|P_{12}\rangle$ or $|P_{13}\rangle$, which are nearly degenerate at this value of the coupling strength, appear as a unique feature around $\omega/\omega_c \approx 3.78$. At $T = 0.15\omega_c/k_B$, extra lines appear as the signature of hot bands. In particular, three transitions arise at ω/ω_c = 3.75 ($|P_2\rangle \rightarrow |P_{23}\rangle$), 3.76 ($|P_2\rangle \rightarrow |P_{24}\rangle$) and 3.82 ($|P_1\rangle \rightarrow |P_{21}\rangle$), near the targeted transition at 3.78ω_c interest, and may interfere with the preparation of the desired initial superposition, making it difficult to prepare the system at this temperature. Hence, for this model system, $k_BT/\omega_c = 0.15$ appears as an approximate upper limit below which the polaritonic states $|P_{12}\rangle$ and $|P_{13}\rangle$ can be superimposed in a coherent way, and above which other polaritonic states coming from hot bands would compromise this coherence.

The IR spectra shown in Fig. 6 are convoluted with a Gaussian function having a width at half maximum of 4 cm^{-1} ($\approx 7.10^{-3}\omega_c$) to mimic the spectral width of a 15 ps laser. Under such conditions, the contributions of polaritonic states $|P_{12}\rangle$ and $|P_{13}\rangle$ cannot be distinguished and both states are therefore excited by the laser pulse. This is consistent with the very small energy gap between these states at $\lambda_c = \lambda_R$ (with the present choice of parameters $\Delta\varepsilon_R \approx 3.5$ cm^{-1}). Therefore, at low temperatures and for an IR excitation using a laser pulse with a spectral width on the order of $\Delta\varepsilon_R$, the initial wavepacket $|\Psi(t=0)\rangle$ can be prepared as $|\Psi(t=0)\rangle \propto \left(\sqrt{R_{0,12}}|P_{12}\rangle + \sqrt{R_{0,13}}|P_{13}\rangle\right)$. Since $R_{0,12} = R_{0,13}$ when $\lambda_c = \lambda_R$, the initial wavepacket $|\Psi(t=0)\rangle$ can be rewritten as a coherent superposition, $|\Psi(t=0)\rangle \simeq \frac{1}{\sqrt{2}}(|P_{12}\rangle + |P_{13}\rangle)$.

The TDSE was numerically solved using this initial condition for γ_2 = 1.0 a.u. as well as other values of γ_2 ranging from half to twice this value, with λ_c being adjusted to the new λ_R according to the values given in Table 3. γ_2 is found to have only little influence on the spectral properties of the polaritonic system; therefore, the above discussion concerning the preparation of the initial state remains valid for other values of this parameter. The resulting time variations of the projected position $\langle q\rangle$ are represented in Fig. 7. Since only two polaritonic states are involved in the initial wavepacket, the time evolution of the system follows a Rabi oscillation. Coherent switching of the wavepacket between the two wells is clearly visible, with a period of about 920 to 2290 $\omega_c t$, *i.e.* 8 to 20 ps, depending on the value of γ_2. The period and the amplitude of the oscillation between the two potential wells both increase with this parameter, as a consequence of the decrease of the energy gap $\Delta\varepsilon_R$ between the two polaritonic eigenstates (see Table 3).

For a molecule having different reactivity properties in the left and right wells, the preparation of such a superposition of polaritonic states near an avoided crossing could be efficiently used to control the outcome of the reaction. However, to exploit such features, experiments would have to be performed at low temperatures and would require damping processes to be minimized on the picosecond time scale, including photon loss inside the cavity and radiative or non-radiative relaxation processes of the molecules.

3.3 Influence of the potential asymmetry

The robustness of the previous analysis was finally investigated by addressing the role of the asymmetry of the double-well potential, which is contained in parameter α_2 of eqn (7). Leaving parameters α_0 and α_1 unchanged, α_2 is divided by 4, leading to a potential with $N_\ell = 4$ and $N_r = 3$ bound states in the left and right parts of the potential, respectively. This alternative potential and the probability densities of its first bound states obtained from solving the Schrödinger equation are depicted in Fig. 8(a). Fixing γ_2 = 0.5 a.u. throughout this section, the eigenenergies of the polaritonic states were determined as a function of the coupling strength λ_c. Partial results represented in Fig. 8(b) highlight the polaritonic states $|P_{10}\rangle$ and $|P_{11}\rangle$, which

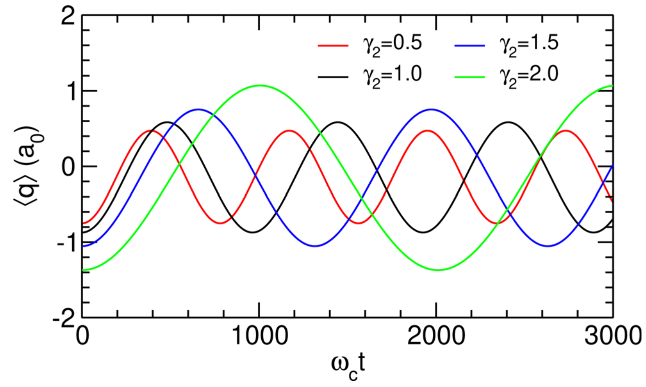

Fig. 7 Projected position $\langle q\rangle$ as a function of time, as obtained for $\lambda_c = \lambda_R$ assuming the initial wavepacket $|\Psi(t=0)\rangle$ given in eqn (16), for different values of γ_2 given in atomic units.

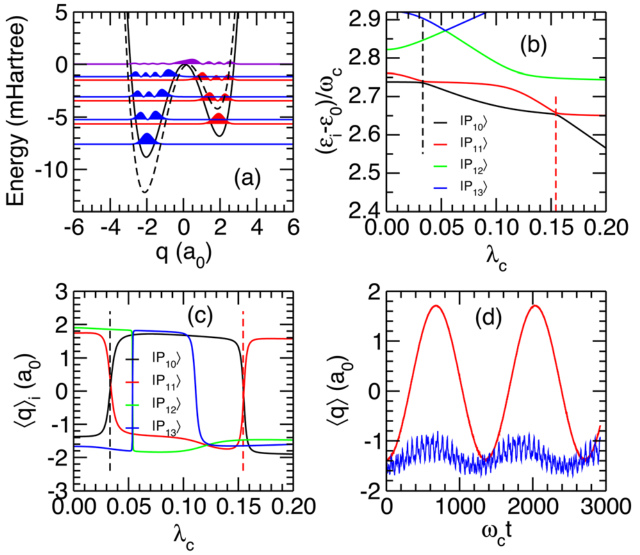

Fig. 8 Results obtained for an alternative double-well potential. (a) Potential energy curve (solid line) and probability densities associated with the lowest eigenstates. For comparison, the previous potential curve is superimposed as a dashed line; (b) relative energies $(\varepsilon_i - \varepsilon_0)/\omega_c$ as a function of the coupling strength λ_c for $|P_{10}\rangle$, $|P_{11}\rangle$, $|P_{12}\rangle$ and $|P_{13}\rangle$; (c) average position $\langle q\rangle_i$ as a function of λ_c for the same polaritonic states; (d) time evolution of $\langle q\rangle$ subsequent to an initial excitation of the uncoupled state $|3_\ell,0\rangle$ for λ_c = 0.033 (red curve) and 0.154 (blue curve).

undergo two avoided crossings at $\lambda_{\rm crit}^{(1)}$ = 0.033 and $\lambda_{\rm crit}^{(2)}$ = 0.154. As shown from the average positions $\langle q\rangle_i$ in Fig. 8(c), these avoided crossings are both connected to transitions in which the system switches between the left and right wells of the potential.

In the limit of vanishing couplings, the polaritonic states $|P_{10}\rangle$ and $|P_{11}\rangle$ can be assigned to the $|3_\ell,0\rangle$ and $|1_r,1\rangle$ states, respectively, while in the vicinity of the two avoided crossings, $|P_{10}\rangle$ and $|P_{11}\rangle$ are mainly decomposed on the uncoupled states $|3_\ell,0\rangle$, $|0_r,2\rangle$ and $|1_r,1\rangle$. Preparing the system in the excited state $v = 3_\ell$ before entering an initially photon-less cavity, leading to an initial state $|3_\ell,0\rangle$, can thus be expected to produce the polaritonic states involved in these avoided crossings. The weights $W_i = |\langle P_i|3_\ell,0\rangle|^2$ of this initial state on the four polaritonic states $|P_i\rangle$, i = 10–13 are reported in Table 4 for the two values of $\lambda_{\rm crit}$. As can be seen in this table, at $\lambda_{\rm crit}^{(1)}$ = 0.033, the two polaritonic states $|P_{10}\rangle$ and $|P_{11}\rangle$ together represent over 99% of the $|3_\ell,0\rangle$ wavepacket, indicating that it can effectively be considered as a linear combination of the polaritonic states $|P_{10}\rangle$ and $|P_{11}\rangle$ alone:

$$|\Psi(t=0)\rangle = |3_\ell,0\rangle \approx \frac{1}{\sqrt{2}}(|P_{10}\rangle + |P_{11}\rangle). \tag{17}$$

Table 4 Weights W_i of state $|3_\ell,0\rangle$ on the four polaritonic states $|P_i\rangle$ with i = 10–13, near the two avoided crossings. Σ corresponds to the sum of these four weights

$\lambda_{\rm crit}$	W_{10}	W_{11}	W_{12}	W_{13}	Σ
0.033	55.0%	44.3%	—	0.5%	99.8%
0.154	6.6%	5.5%	78.1%	7.5%	97.7%

The time evolution obtained after preparing the system in this initial state at $\lambda_c = \lambda_{\rm crit}^{(1)}$ is represented in Fig. 8(d). A Rabi oscillation between the left and right wells is found at a period of about 1600 $\omega_c t$ (about 14 ps), with an amplitude that indicates an efficient coherent switching between the polaritonic states $|P_{10}\rangle$ and $|P_{11}\rangle$.

For the second avoided crossing at $\lambda_{\rm crit}^{(2)}$ = 0.154, the $|3_\ell,0\rangle$ state is no longer a superposition of the polaritonic states $|P_{10}\rangle$ and $|P_{11}\rangle$ as it now mainly involves $|P_{12}\rangle$ and has a non negligible weight on $|P_{13}\rangle$. In the limit of vanishing couplings, the polaritonic states $|P_{12}\rangle$ and $|P_{13}\rangle$ can be assigned to the $|0_r,2\rangle$ and $|2_\ell,1\rangle$ states, respectively. However, near $\lambda_{\rm crit}^{(2)}$, the energy of $|P_{12}\rangle$ approaches the energy of the initially prepared $|3_\ell,0\rangle$ state, therefore explaining the large weight of this state on $|P_{12}\rangle$. The average positions of $|P_{12}\rangle$ and $|P_{13}\rangle$ displayed in Fig. 8(c) show that both polaritonic states reside in the left well near $\lambda_{\rm crit}^{(2)}$ ($\langle q\rangle_i < 0$ for i = 12, 13). Hence, it is not surprising that no significant switching between the wells is found near this avoided crossing, as confirmed by the temporal evolution of $\langle q\rangle(t)$ in Fig. 8(d).

4 Conclusion and perspectives

The strong interaction between a one-dimensional potential mimicking a bistable molecular system and a single-mode Fabry–Perot microcavity, leading to the formation of quantum polaritonic states, was computationally investigated using simple double-well potential and dipole moment models. Although largely phenomenological in nature, the present model aims to describe a flexible molecule or a reactive system undergoing intramolecular rearrangement such as proton transfer and is rather generic in this respect.

Considering a cavity in resonance with the first vibrational transition, a rich phenomenology of polaritonic states was suggested by tuning the light–matter coupling strength around polaritonic avoided crossings, thereby exploring the idea of vacuum-modified chemistry. The possibility of coherently switching the molecular system between the two potential wells near avoided crossings that involve polaritonic states located in either well of the potential was theoretically demonstrated.

Two possible ways of inducing coherent state switching were considered. First with the preparation of the free molecule in a specific vibrational state before its insertion inside a cavity not containing any photon, as it could be achieved using a molecular beam perpendicular to the cavity. Alternatively, and assuming that (non-interacting) molecules are in thermal equilibrium inside the cavity, a suitable excitation by a picosecond laser of a wavepacket mixing two polaritonic states could also lead to coherent switching and produce a Rabi-like oscillation between the left and right wells. The robustness of these results with respect to the potential asymmetry and dipole parameters has been thoroughly studied.

The switching time was found to depend significantly on the details of the system, including the potential itself but also the dipole moment function. Although the focus was on non-polar states, the dipole moment function plays a key role in polaritonic chemistry[35,38] and it would be worth extending the model to the cases where either of the states, if not both, are polar. More generally, the model could be made more realistic with the goal of opening more perspectives toward the measurement of some of the predicted effects and contributing to addressing the somewhat controversial field of polaritonic chemistry. One natural extension would be to focus on polyatomic molecules, starting with the triatomic case, and explore the possibility of transferring energy across vibrational modes by selectively playing on some polaritonic avoided crossings. Since the reactivity of polyatomic molecules might be enhanced when specific vibrational modes are excited, the coupling of the molecule with the confined light of the microcavity could lead to controlled reactivity.

Author contributions

Loïse Attal: conceptualization (equal), investigation (supporting), software (supporting), validation (equal), writing – original draft (lead), writing – review & editing (equal); Florent Calvo: conceptualization (equal), validation (equal), visualization (supporting), writing – original draft (supporting), writing – review & editing (equal); Cyril Falvo: conceptualization (equal), validation (equal), writing – original draft (supporting), writing – review & editing (equal); Pascal Parneix: conceptualization (equal), investigation (lead), software (lead), supervision (lead), validation (equal), visualization (lead), writing – original draft (lead), writing – review & editing (equal).

Conflicts of interest

There are no conflicts to declare.

Acknowledgements

The authors acknowledge financial support from GDR EMIE 3533. L. A. acknowledges financial support from MESRI through a PhD fellowship granted by the EDOM doctoral school.

Notes and references

1 T. Schwartz, J. Hutchison, C. Genet and T. Ebbesen, *Phys. Rev. Lett.*, 2011, **106**, 196405.
2 J. Hutchison, T. Schwartz, C. Genet, E. Devaux and T. Ebbesen, *Angew. Chem., Int. Ed.*, 2012, **6**, 1592–1596.
3 S. Wang, A. Mika, J. A. Hutchison, C. Genet, A. J. M. W. Hosseini and T. Ebbesen, *Nanoscale*, 2014, **6**, 7243–7248.
4 J. P. Long and B. S. Simpkins, *ACS Photonics*, 2015, **2**, 130–136.
5 B. S. Simpkins, K. Fears, W. Dressick, B. T. Spann, A. Dunkelberger and J. C. Owrutsky, *ACS Photonics*, 2015, **2**, 1460–1467.
6 J. Flick, N. Rivera and P. Nareng, *Nanophotonics*, 2018, **7**, 1479–1501.
7 R. F. Ribeiro, L. A. Martinez-Martinez, M. Du, J. Campos-Gonzalez-Angulo and J. Yuen-Zhou, *Chem. Sci.*, 2018, **9**, 6325–6339.
8 A. Thomas, L. Lethuillier-Karl, K. Nagarajan, R. M. A. Vergauwe, J. George, T. Chervy, A. Shalabney, E. Devaux, C. Genet, J. Moran and T. W. Ebbesen, *Science*, 2019, **363**, 615–619.
9 T. E. Li, A. Nitzan and J. E. Subotnik, *Angew. Chem.*, 2021, **133**, 15661–15668.
10 X. Li, A. Mandal and P. Huo, *J. Phys. Chem. Lett.*, 2021, **12**, 6974–6982.
11 A. Shalabney, J. George, H. Hiura, J. A. Hutchison, C. Genet, P. Hellwig and T. Ebbesen, *Angew. Chem., Int. Ed.*, 2015, **54**, 7971–7975.
12 A. Thomas, J. George, A. Shalabney, M. Dryzhakov, S. Varma, J. Moran, T. Chervy, X. Zhong, E. Devaux, C. Genet, J. Hutchison and T. W. Ebbesen, *Angew. Chem.*, 2016, **128**, 11634–11638.
13 W. M. Takele, F. Wackenhut, L. Piatkowski, A. J. Meixner and J. Waluk, *J. Phys. Chem. B*, 2020, **124**, 5709–5716.
14 A. D. Wright, J. C. Nelson and M. L. Weichman, *J. Am. Chem. Soc.*, 2023, **145**, 5982–5987.
15 J. George, A. Shalabney, J. A. Hutchison, C. Genet and T. W. Ebbesen, *J. Phys. Chem. Lett.*, 2015, **6**, 1027–1031.
16 J. del Pino, J. Feist and F. J. Garcia-Vidal, *J. Phys. Chem. C*, 2015, **119**, 29132–29137.
17 A. Strashko and J. Keeling, *Phys. Rev. A*, 2016, **94**, 023843.
18 W. Ahn and B. S. Simpkins, *J. Phys. Chem. C*, 2021, **125**, 830–835.
19 P. Saurabh and S. Mukamel, *J. Chem. Phys.*, 2016, **144**, 124115.
20 B. Cohn, S. Sufrin and L. Chuntonov, *J. Chem. Phys.*, 2022, **156**, 121101.
21 X. Xiong, *Acc. Chem. Res.*, 2023, **56**, 776–786.
22 J. George, T. Chervy, A. Shalabney, E. Devaux, H. Hiura, C. Genet and T. W. Ebbesen, *Phys. Rev. Lett.*, 2016, **117**, 153601.
23 M. Muallem, A. Palatnik, G. D. Nessim and Y. Tischler, *J. Phys. Chem. Lett.*, 2016, **7**, 2002–2008.
24 R. M. A. Vergauwe, J. George, T. Chervy, J. A. Hutchison, A. Shalabney, V. Y. Torbeev and T. W. Ebbesen, *J. Phys. Chem. Lett.*, 2016, **7**, 4159–4164.
25 O. Kapon, R. Yitzhari, A. Palatnik and Y. R. Tischler, *J. Phys. Chem. C*, 2017, **121**, 18845–18853.
26 S. Takahashi, K. Watanabe and Y. Matsumoto, *J. Chem. Phys.*, 2019, **151**, 074703.
27 B. S. Simpkins, A. D. Dunkerberger and J. C. Owrutsky, *J. Phys. Chem. C*, 2021, **125**, 19081–19087.
28 M. V. Imperatore, J. B. Asbury and N. C. Giebink, *J. Chem. Phys.*, 2021, **154**, 191103.
29 G. D. Wiesehan and W. Xiong, *J. Chem. Phys.*, 2021, **155**, 211103.
30 P. A. Thomas, W. J. Tan, V. G. Kravets, A. N. Grigorenko and W. L. Barnes, *Adv. Mater.*, 2023, 2309393, in press.
31 M. Tavis and F. W. Cummings, *Phys. Rev.*, 1968, **170**, 379–384.
32 G. Groenhof and J. J. Toppari, *J. Phys. Chem. Lett.*, 2018, **9**, 4848–4851.

33 R. F. Ribeiro, A. D. Dunkelberger, B. Xiang, W. Xiong, B. Simpkins, J. Owrutsky and J. Yuen-Zhou, *J. Phys. Chem. Lett.*, 2018, **9**, 3766–3771.

34 F. J. Hernandez and F. Herrera, *J. Chem. Phys.*, 2019, **151**, 144116.

35 J. F. Triana, F. J. Hernandez and F. Herrera, *J. Chem. Phys.*, 2020, **152**, 234111.

36 F. Herrera and J. Owrutsky, *J. Chem. Phys.*, 2020, **152**, 100902.

37 E. W. Fischer and P. Saalfrank, *J. Chem. Phys.*, 2020, **154**, 104311.

38 J. F. Triana and J. L. Sanz-Vicario, *J. Chem. Phys.*, 2021, **154**, 094120.

39 T. E. Li, A. Nitzan and J. E. Subotnik, *J. Chem. Phys.*, 2021, **154**, 094124.

40 D. S. Wang and S. F. Yelin, *ACS Photonics*, 2021, **8**, 2818–2826.

41 E. W. Fischer and P. Saalfrank, *J. Chem. Phys.*, 2022, **157**, 034305.

42 A. Mandal, X. Li and P. Huo, *J. Chem. Phys.*, 2022, **156**, 014101.

43 J. A. Gòmez and O. Vendrell, *J. Phys. Chem. A*, 2023, **127**, 1598–1608.

44 E. W. Fischer, J. Anders and P. Saalfrank, *J. Chem. Phys.*, 2022, **156**, 154305.

45 M. Balasubrahmaniyam, C. Genet and T. Schwartz, *Phys. Rev. B*, 2021, **103**, L241407.

46 A. Mandal, D. Xu, A. Mahajan, J. Lee, M. Delor and D. R. Reichman, *Nano Lett.*, 2023, **23**, 4082–4089.

47 I. S. Ulusoy, J. A. Gomez and O. Vendrell, *J. Phys. Chem. A*, 2019, **123**, 8832–8844.

48 T. Schnappinger, D. Sidler, M. Ruggenthaler, A. Rubio and M. Kowalewski, *J. Phys. Chem. Lett.*, 2023, **14**, 8024–8033.

49 T. Schnappinger and M. Kowalewski, *J. Chem. Theory Comput.*, 2023, **19**, 9278–9289.

50 W. Pauli and M. Fierz, *Nuovo Cimento*, 1938, **15**, 167–188.

51 J. V. Lill, G. A. Parker and J. Light, *Chem. Phys. Lett.*, 1982, **89**, 483–489.

52 J. V. Lill, G. A. Parker and J. Light, *J. Chem. Phys.*, 1985, **85**, 900–910.